

Multiple-slice imaging of a tissue-equivalent phantom by use of time-resolved optical tomography

Florian E. W. Schmidt, Jeremy C. Hebden, Elizabeth M. C. Hillman, Martin E. Fry, Martin Schweiger, Hamid Dehghani, David T. Delpy, and Simon R. Arridge

Following several years of development the construction of a multichannel time-resolved imaging device for medical optical tomography has been completed. Images are reconstructed from time-resolved measurements by use of a scheme that employs a finite-element diffusion-based forward model and an iterative reconstruction solver. Prior to testing on clinical subjects the fully automated instrument and the reconstruction software are evaluated with tissue-equivalent phantoms. We describe our first attempt to generate multiple-slice images of a phantom without uniform properties along the axial direction, while still using a computationally fast two-dimensional reconstruction algorithm. The image quality is improved by the employment of an approximate correction method that uses scaling factors derived from the ratios of finite-element forward simulations in two and three spatial dimensions. The 32-channel system was employed to generate maps of the internal scattering and the absorption properties at 14 different transverse planes across the phantom. The images clearly reveal the locations of small inhomogeneous regions embedded within the phantom. These results were obtained by use of purely temporal data and without recourse to reference measurements. © 2000 Optical Society of America

OCIS codes: 170.3010, 170.6920, 170.6960, 170.0110.

1. Introduction

The idea, first demonstrated in 1977 by Jöbsis,¹ that differences in the characteristic absorption by the oxygenated and the deoxygenated forms of hemoglobin at optical wavelengths can be exploited as a means of diagnosing tissue function has motivated the rapid evolution of the field known as biomedical optics.²⁻⁵ At University College London (UCL) there has been particular interest in the potential of optical radiation for studying brain function in the human neonate. Early detection of abnormal cerebral oxygenation or perfusion could lead to the prevention of permanent brain injury. A continuous bedside imaging device, which can be operated in an

intensive care unit, may therefore represent a useful tool for diagnosing hypoxic ischemia in premature infants and conditions resulting from birth asphyxia in term infants.

The development of optical tomography has been a principal focus of biomedical optics research at UCL and elsewhere. Unlike the conventional tomography employed in x-ray and other established medical imaging modalities, reconstruction must utilize measurements of radiation that has been diffusely transmitted. Therefore the Radon transform and the backprojection methods are generally not applicable. Nevertheless, optical tomography relies on the assumption that a finite set of measurements of transmitted light between pairs of points on the surface of an object is sufficient to reconstruct an arbitrary three-dimensional (3-D) distribution of internal scatterers and absorbers.

The approach we have pursued, as manifested by the reconstruction package known as temporal optical absorption and scattering tomography (TOAST), is to determine the parameters that describe an appropriate model of photon migration within the object by comparing its predictions with the measured data. The model is then adjusted iteratively to minimize the difference between the two. TOAST contains three distinct components: (i) a finite-element

When this research was performed, the authors were with University College London. F. E. W. Schmidt, J. C. Hebden, E. M. C. Hillman, M. E. Fry, M. Schweiger, H. Dehghani, and D. T. Delpy were with the Department of Medical Physics, 11-20 Capper Street, London WC1E 6JA, United Kingdom. S. R. Arridge is with the Department of Computer Science, Gower Street, London WC1E 6BT, United Kingdom. F. E. W. Schmidt is now with P. A. Consulting Group, London SW1W 9SR, United Kingdom.

Received 12 October 1999; revised manuscript received 14 March 2000.

0003-6935/00/03380-08\$15.00/0

© 2000 Optical Society of America

method (FEM) forward model from which to generate simulated measurements for a given distribution of internal scattering and absorbing properties, (ii) the definition of an objective function to be minimized based on the error between model predictions and experimental data, and (iii) a scheme for adjusting the parameters of the forward model to achieve the minimization.^{6,7}

A variety of reconstruction schemes have been proposed by other research groups. Pogue *et al.*⁸ described a method that employs frequency-domain difference data [i.e., data recorded with and without perturbing object(s) present]. Continuous intensity measurements on phantoms were used by Jiang *et al.*⁹ to obtain maps of absorption and scattering objects, whereas Ueda *et al.*¹⁰ reported reconstructions of absorption images from absolute intensity measurements without any reference data. Meanwhile, Ntziachristos *et al.*¹¹ extracted discrete frequencies from the Fourier transform of time-resolved difference measurements to obtain absorption and scattering images of breast phantoms.

Although apparently simple to acquire, the absolute intensity of light transmitted between two points on the surface of a scattering object is not considered a feasible measurement for clinical optical tomography in practice because of the overwhelming influence of photon-tissue interactions very close to the tissue surface.¹² Thus many investigators have sought to develop instruments that perform measurements in the time or the frequency domain. The former measure the temporal distribution of photons transmitted between points on the surface in response to illumination by an impulse of light,^{11,13–15} whereas the latter determine the modulation amplitude and the phase delay in response to an intensity-modulated signal.^{16–18} The potentially critical information content at higher (>1 -GHz) frequencies gives time-domain measurements a significant advantage in terms of the availability of suitable instrumentation, and therefore it was decided at UCL to develop an imaging system based on state-of-the-art time-correlated single-photon-counting instrumentation. After several years of development construction of the imager was recently completed and is described in detail by Schmidt *et al.*¹⁹

The UCL system, known as MONSTIR (multichannel optoelectronic near-infrared system for time-resolved image reconstruction), is illustrated schematically in Fig. 1. A beam of picosecond pulses from a Ti:sapphire laser operated at a repetition rate of approximately 80 MHz and a wavelength of 800 nm is coupled sequentially by means of optical fibers to the surface of the object. Transmitted light is collected simultaneously by 32 detector fiber bundles. These bundles deliver the light to four 8-anode microchannel-plate photomultiplier tubes (MCP-PMT's) through 32 variable optical attenuators (VOA's) that ensure that the intensity of detected light does not saturate or damage the MCP-PMT's. Each detected photon results in an electronic pulse whose arrival time is measured with respect to a

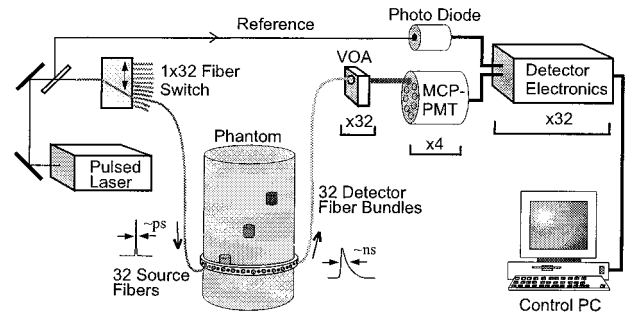


Fig. 1. Schematic of the 32-channel time-resolved imaging system MONSTIR.

laser-generated reference signal, and histograms of photon flight times [the so-called temporal point-spread functions (TPSF's)]-are accumulated. The full set of TPSF's is subsequently transferred to a dedicated workstation for image reconstruction.

Prior to completion of the instrument the performance of MONSTIR was evaluated by use of an 8-channel (single-MCP-PMT) configuration. As was described elsewhere,²⁰ eight detector bundles and two source fibers were arranged around the circumference of a solid tissue-equivalent phantom, and by manual rotation of the ring around the phantom data that were equivalent to those from 16 source fibers and 16 detectors were acquired. The data were then successfully employed to reconstruct two maps representing the distribution of scatter and absorption within the transverse plane. A feature of this previously reported research was a reliance on phantoms with uniform properties along the axial direction on the basis of an assumption that they were more likely to yield satisfactory images from a two-dimensional (2-D) forward model (although a 2-D model is strictly valid in this case only if the source is also infinite along the axial direction). Although TOAST has the facility to employ fully 3-D FEM models, the computational demands are much greater than for 2-D models, and therefore the latter are attractive.

The research presented here was motivated by a desire to increase the domain of the 2-D modeling scheme—with its inherent advantages of reconstruction speed—by investigation of its application to objects without axial uniformity. An attempt was made to reconstruct the absorption and the scattering properties within different transverse planes of a nonuniform cylindrical phantom by the positioning of a ring of sources and detectors at different heights along the cylinder's axis. By use of a method described below in Section 3, the time-resolved measurements acquired for each plane are adjusted to provide an approximate compensation for the expected differences between data generated by the 2-D and the 3-D forward models.

2. Method

A recipe developed by Firbank *et al.*²¹ was employed to produce a solid tissue-equivalent phantom in the

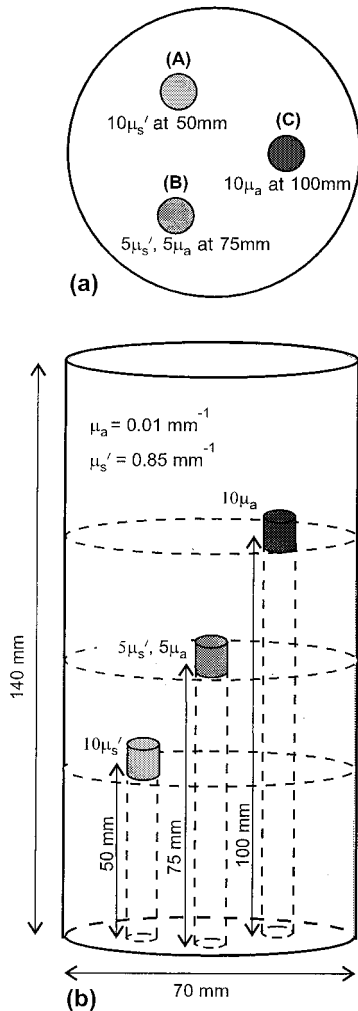


Fig. 2. Schematic diagram of the cylindrical solid tissue-equivalent phantom: (a) top view and (b) front view.

form of a cylindrical block, 140 mm in length and 70 mm in diameter, as illustrated in Fig. 2. The block has a nominal transport-scatter coefficient of $\mu'_s = 0.85 \pm 0.10 \text{ mm}^{-1}$ and an absorption coefficient of $\mu_a = 0.010 \pm 0.002 \text{ mm}^{-1}$ at a wavelength of 780 nm. Inserted within the block are three small cylinders that are 10 mm in length and 8 mm in diameter. Each is centered 17.5 mm from the central axis at different heights from the base: 50 mm (cylinder A), 75 mm (cylinder B), and 100 mm (cylinder C). The three cylinders were constructed with relative optical coefficients of $10\mu'_s$ and μ_a , $5\mu'_s$ and $5\mu_a$, and μ'_s and $10\mu_a$, respectively. The scatter is varied according to different concentrations of titanium dioxide particles, and absorption depends on the amount of an appropriate near-infrared dye. The variation in the titanium dioxide concentration also provides a small degree of x-ray contrast, and thus the precise locations of cylinders A and B could be confirmed by use of x-ray computed tomography.

Thirty-two detector fiber bundles and 32 source fibers are held in contact with the surface by use of a black plastic ring that fits around the circumference

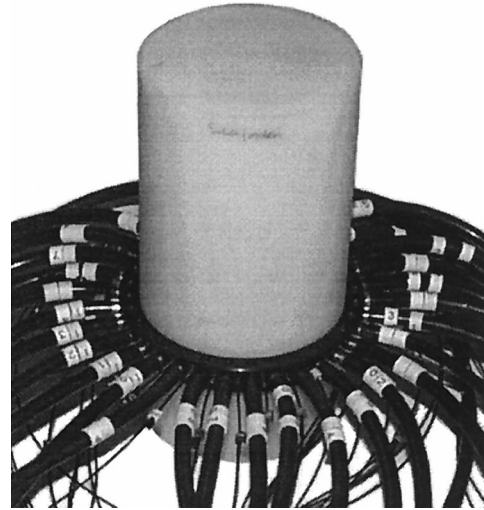


Fig. 3. Photograph of the cylindrical phantom and the fiber holder ring.

of the phantom. A photograph of the fiber assembly and the phantom is shown in Fig. 3. Data were recorded with the ring located at 14 different heights at intervals of 5 mm between 40 mm and 105 mm above the base. The preprogrammed data-acquisition protocol was performed automatically under computer control for each configuration, and the VOA's ensured that the photon-count rates for each detector did not exceed approximately 3×10^5 photons/s. Because of the high signal detected for the shortest optode separations, five detectors on either side of each source had to be deactivated by the switching of the VOA's to zero transmission. However, such measurements are expected to contribute little to the reconstruction of deeper structure within the object. The acquisition geometry can therefore be considered to be a rotating fan beam such as is commonly employed in other manifestations of tomography.

Data were recorded by each activated detector simultaneously for 15 s for each source position, and the resulting 32×22 TPSF's were stored on the system PC for each of the 14 ring positions. The variability in absolute temporal delay that was due to the different lengths of source fibers, detector bundles, and electronic cables was precalibrated by use of procedures outlined elsewhere.¹⁹ As a consequence of the desire to reduce data redundancy and minimize the forward-model calculation, TOAST accommodates data in the form of various characteristics of the measured TPSF's. These so-called data types currently can consist of any combination of temporal moments (around zero), central moments (around the mean), normalized Laplace and Mellin-Laplace transforms, and integrated intensity.²²

For this experiment three data types were derived from each TPSF: the mean flight time, the variance about the mean, and the Laplace transform (with a coefficient of 0.005 ps^{-1}). The effect of the finite temporal response of the system on each TPSF was

corrected by use of measurements of the instrument response function that were recorded for all channels and appropriate correction procedures, as described by Hillman *et al.*²³ Occasionally an individual detector channel exhibited evidence of temporal instability, and the corresponding data were removed.

3. Two-Dimensional–Three-Dimensional Compensation

When all sources and detectors are confined to a single plane in a geometry resembling conventional x-ray tomography it is tempting to suppose that reconstruction could be achieved by use of an algorithm that would likewise be limited to two dimensions. However, because photons migrate in all three dimensions in a scattering medium, measurements made at the surface are inevitably sensitive to structure located above and below the plane of interest. Although this sensitivity will decrease quite rapidly with increasing distance from the plane, reconstruction must employ a 3-D forward model if quantitative imaging is required. Furthermore, the statistical distribution of photon flight times between two points for 2-D and 3-D models are sufficiently dissimilar as to produce a significant difference in the forward-model predictions of the TPSF. Nevertheless, as was described in Section 2, 2-D models are very attractive because of the substantially faster computation. Therefore we investigated whether it is possible to apply an appropriate correction to experimental data to render them more suitable for a 2-D algorithm. This idea was previously explored by use of data that were simulated with a 3-D FEM model, and results were obtained that revealed fewer artifacts and greater clarity than were achieved without such a correction.²⁴

Correction involves rescaling each data type by a factor that is dependent on the source–detector separation. As was proposed by Schweiger *et al.*,²⁴ the scaling factors are equal to the ratio of the data types computed from the 2-D and the 3-D FEM simulations by use of a homogenous object with the same physical geometry and average optical properties. The average optical properties of the phantom employed here, although known *a priori* with reasonable confidence, were estimated by use of an infinite-space Green's function model to find values of μ_a and μ'_s that were consistent with the average values of all three data types (mean, variance, Laplace) for large (>50 -mm) source–detector separations for a single plane. The values obtained were $\mu'_s = 0.85 \text{ mm}^{-1}$ and $\mu_a = 0.011 \text{ mm}^{-1}$. The same data types at the same source–detector separations were then computed from FEM simulations based on a 2-D circular and a 3-D cylindrical mesh.

Good agreement between the average data types and the 3-D model values confirmed the accuracy of the average-value computation. Scaling factors were then calculated for each data type and separation by the division of the 2-D model value by the 3-D model value. Each data type that was extracted from the experimental data was multiplied by the appropriate scaling factor prior to its use in a 2-D

reconstruction algorithm. The computation of the scaling factors, the estimation of the average properties, and the other correction procedures mentioned in Section 2 are described in much greater detail by Hillman *et al.*²³ Although this 2-D–3-D correction method does not circumvent the problem of the influence of out-of-plane structure on the recorded data, the results presented in Section 4 suggest that it does provide a reasonable *ad hoc* method of reducing the distortion in the forward-model predictions that arise from the use of a 2-D mesh.

4. Results

The TOAST image-reconstruction package was employed to derive simultaneous maps of the absorbing and the scattering properties from the 2-D–3-D compensated data for each of the 14 ring positions. The software was also provided with the coordinates of the surface locations of each source and detector in the ring and with a circular FEM mesh that consisted of 7392 triangular elements. At each iteration step search directions and step lengths were computed by use of a nonlinear conjugate-gradient method with median filtering after each update.²⁵

The 2-D reconstruction scheme required approximately 200 s/iteration on a Pentium PC, which is more than an order of magnitude faster than would have been required for a full 3-D simultaneous reconstruction from the same data with a 3-D FEM mesh of similar element density. The initial iteration is simply a backprojection of the model–data mismatch and is very smooth. Subsequent iterations show improved resolution and contrast at the expense of introducing image artifacts. An increasing dominance of artifacts is a characteristic feature of iterative image reconstruction, but their effect here is more dominant than is seen in simulations because of the presence of systematic measurement errors. Hardware modifications and improved calibration methods are being introduced to decrease or eliminate residual systematic errors, and appropriate regularization schemes, as described by Arridge *et al.*,²⁶ may also help to reduce artifacts in the future.

Images for each of the 14 ring positions are shown in Fig. 4. They are a compromise between quantitative accuracy and artifacts, and both sets of 14 images are displayed such that a given gray level corresponds to the same reconstructed value of the absorption or the transport-scatter coefficient. The range of displayed values is 0.010 – 0.012 mm^{-1} for μ_a and 0.73 – 1.08 mm^{-1} for μ'_s .

The three embedded cylinders appear with highest contrast in the planes in which they are known to be centered, and each is apparent in the two adjacent planes on either side of the centered plane, indicating that their influence in the vertical direction extends at least 5 mm beyond their physical dimensions. Transverse and vertical cross sections of the purely absorbing and the purely scattering cylinders C and A, respectively, are shown in Fig. 5. The transverse (radial) FWHM values are $\sim 17.5 \text{ mm}$ and $\sim 12.2 \text{ mm}$ for the absorber and the scatterer, respectively. If

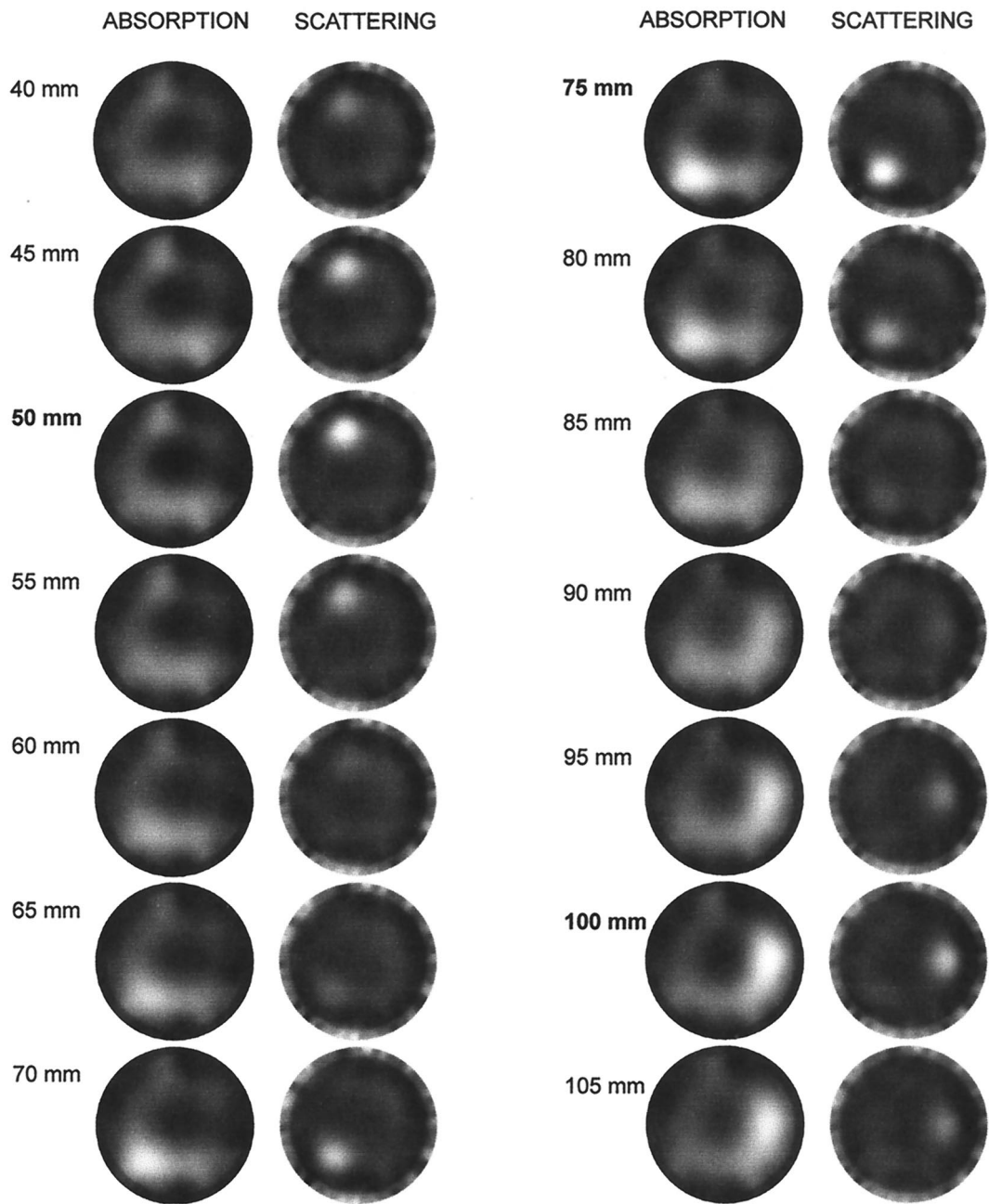


Fig. 4. Reconstructed absorption and scattering maps for 14 different cross-sectional planes along the phantom.

the finite diameter (8 mm) of the cylinders is taken into account these numbers provide a rough measure for the transverse spatial resolutions in these images of approximately 16 and 9 mm, respectively. (We estimate the spatial resolution by assuming that the point-spread functions and the cylinder widths add in quadrature to produce the measured width.)

Many factors influence the spatial resolution. These include the optical properties and the dimensions of the phantom, the depth of the structure beneath the boundary, and the data types and the quality of the data employed. Note the slight error in the transverse positions of cylinders C and A [Fig. 5(a) and 5(c), respectively], which appear to be shifted

by ≤ 2 mm. However, this error is small compared with the width of the curve. The plots of the depth profiles do not allow an exact estimate of the vertical FWHM to be made because the lowest and the highest planes acquired in this scan are just below and above, respectively, cylinders A and C. Nevertheless, if symmetry of the peaks is assumed, it is evident that the vertical FWHM of the scattering cylinder is comparable with that of the transverse case, whereas that for the absorber appears to be somewhat broader. However, these vertical resolutions are remarkably good, given that each image slice represents an entirely independent 2-D reconstruction.

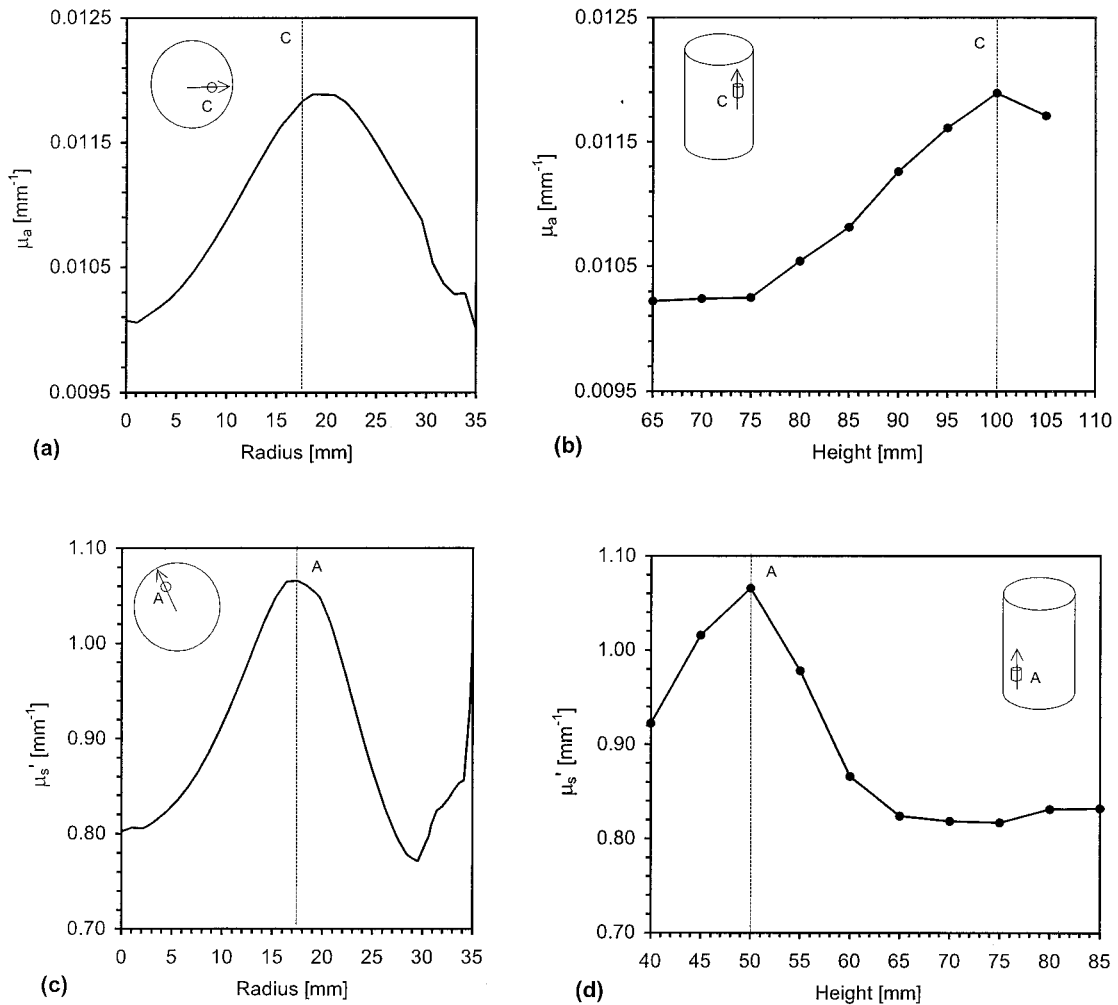


Fig. 5. (a) Transverse and (b) vertical cross sections of the purely absorbing cylinder C, which was centered at 100 mm above the base. Corresponding (c) transverse and (d) vertical cross sections of the purely scattering cylinder A, which was centered at 50 mm above the base. Note that the vertical cross sections consist of one data point per slice.

The spatial resolution exhibited in the absorbing images is, as was previously observed,²⁰ significantly poorer than that exhibited in the scattering images; this result reflects the comparatively weak dependence of a perturbation in absorption on the time-of-flight measurements. Ideally, we would use the absolute detected intensity as an additional measurable, but at present this seems impractical given this element's strong dependence on surface interactions and without the use of a reference measurement.

As Fig. 5 indicates, the contrasts of the purely absorbing and the purely scattering cylinders are only approximately 20% and 30%, respectively, i.e., they are significantly less than the nominal $\times 10$ object-to-background ratio. Although the overall quality of the images quickly degrades with further iteration because of the increased dominance of artifacts, we observe that the contrast of the embedded cylinders also increases. It is likely that our ongoing efforts to decrease the incidence of artifacts caused by residual systematic measurement errors will facilitate better quality images at larger iterations in which the fea-

ture contrast is much greater. However, the reconstructed values of the embedded cylinders are not expected to be quantitatively accurate without using a 3-D forward model. The finite spatial resolution is also expected to have a significant effect on the absolute quantitation because the volumes of the reconstructed features, which are estimated by use of the FWHM dimensions, are of the order of 5 times greater than the volumes of the embedded objects. Other authors have reported more quantitatively accurate results^{8,11} that are, however, based on difference imaging, which cancels out many of these sources of uncertainty.

The absorption and the scattering maps reveal reasonable separation between the properties of the embedded cylinders. There is little evidence of the scattering cylinder in the absorption images (centered at 50 mm) but some stronger evidence of the absorbing cylinder in the scattering images (centered at 100 mm). This so-called cross talk is an inevitable consequence of the lack of orthogonality in the dependency of the chosen data types on both optical

parameters, as was previously demonstrated by Schweiger and Arridge.²²

A few relatively minor artifacts are present in the images. Both sets of images exhibit a low-power ring artifact, although, as described by Hillman *et al.*,²³ this is substantially reduced by the employment of the 2-D–3-D correction method. The scattering images also exhibit an irregular intensity variation around the boundary [see also Fig. 5(c)], which possibly is due to insufficiently accurate modeling of the true source distribution near the surface, residual systematic error, or both. The faint but sharply defined ring at the boundary of the scattering profile is largely a meshing artifact and is a consequence of the fact that the image is reconstructed into an element basis.

5. Discussion

The results presented above have demonstrated that it is possible to reconstruct transverse images of objects by use of a 2-D reconstruction scheme, even when the object is not uniform along the axial direction. The advantage in terms of reconstruction speed is enormous. Despite the simplicity of the 2-D–3-D data-compensation method, these results have demonstrated the capability of reconstructing images that allow absorption and scattering objects to be localized and discriminated. Nevertheless, the approximate nature of this correction together with residual systematic errors in the data-acquisition process pose a limit on the quality of the reconstructed images.

A very important feature of the research presented here is the use of purely temporal (as opposed to intensity) data and the lack of dependence on any kind of reference measurement. A common approach to optical tomography is to derive difference images, which entails acquiring data from the object in two different states in which the features of interest have modified optical properties. This derivation is easily achieved for simple phantoms by the recording of data with and without a perturbing region inserted into an otherwise homogeneous medium.^{8,9,11} For tissue imaging the spectral dependence of absorption could be exploited to provide some degree of contrast in data that are acquired at two wavelengths. However, the capability of performing optical tomography without reference or difference data, as has been exhibited here, is likely to be of significant benefit.

The ultimate aim of our optical tomography research is to acquire images with absolute quantitation of absorption and scatter, and, in this respect, 2-D reconstruction methods are clearly not appropriate. This is obvious if the embedded object does not have longitudinal symmetry, and, even if it does, no simple correction method can compensate for the influence of out-of-plane structure on the recorded data. The use of a 3-D forward model is essential, and 3-D reconstruction methods are currently being tested by this research group.²⁷ As we have completed the development of the imaging instrument and obtained

encouraging results from increasingly complex tissue-equivalent phantoms, our efforts now are focused on performing preliminary clinical studies. The results discussed here indicate that single-slice 2-D–3-D corrected imaging of the neonatal head, whereby the source and the detector fibers are arranged in a single plane, may be feasible, although without expectation of quantitative images.

To facilitate and encourage the comparison of various imaging techniques that are being pursued within the biomedical optics community, we have made our data, phantoms, and software available through our website: <http://www.medphys.ucl.ac.uk/research/borg>.

The authors thank Peter Mardsen for performing the x-ray computed-tomography measurements on the phantom. Support for this research has generously been provided by Wellcome Trust and Hamamatsu Photonics. F. Schmidt gratefully acknowledges the support of a UCL graduate school scholarship.

References

1. F. F. Jöbsis, "Noninvasive, infrared monitoring of cerebral and myocardial oxygen sufficiency and circulatory parameters," *Science* **198**, 1264–1267 (1977).
2. B. Chance, R. R. Alfano, and B. J. Tromberg, eds., *Optical Tomography and Spectroscopy of Tissue III*, Proc. SPIE **3597** (1999).
3. J. G. Fujimoto and M. S. Patterson, eds., *Advances in Optical Imaging and Photon Migration*, Vol. 21 of OSA Trends in Optics and Photonics Series (Optical Society of America, Washington, D.C., 1998).
4. B. Chance, C. E. Cooper, D. T. Delpy, and E. O. R. Reynolds, eds., *Feature Issue on Near-Infrared Spectroscopy and Imaging of Living Systems*, Philos. Trans. R. Soc. London B **352**, 649–763 (1997).
5. B. Tromberg, A. Yodh, E. Sevick, and D. Pine, eds., *Feature Issue on Diffusing Photons in Turbid Media*, Appl. Opt. **36**, 9–231 (1997).
6. M. Schweiger and S. R. Arridge, "A system for solving the forward and inverse problems in optical spectroscopy and imaging," in *Advances in Optical Imaging and Photon Migration*, R. R. Alfano and J. G. Fujimoto, eds., Vol. 2 of OSA Trends in Optics and Photonics Series (Optical Society of America, Washington, D.C., 1996), pp. 263–268.
7. S. R. Arridge, "Optical tomography in medical imaging," *Inverse Probl.* **15**, R41–R93 (1999).
8. B. W. Pogue, M. S. Patterson, H. Jiang, and K. D. Paulsen, "Initial assessment of a simple system for frequency domain diffuse optical tomography," *Phys. Med. Biol.* **40**, 1709–1729 (1995).
9. H. Jiang, K. D. Paulsen, U. L. Osterberg, and M. S. Patterson, "Improved continuous light diffusion imaging in single- and multi-target tissue-like phantoms," *Phys. Med. Biol.* **43**, 675–693 (1998).
10. Y. Ueda, K. Ohta, M. Oda, M. Miwa, Y. Yamashita, and Y. Tsuchiya, "Average value method: a new approach to practical optical computed tomography for a turbid medium such as human tissue," *Jpn. J. Appl. Phys.* **37**, 2717–2723 (1998).
11. V. Ntziachristos, X. Ma, and B. Chance, "Time-correlated single photon counting imager for simultaneous magnetic resonance and near-infrared mammography," *Rev. Sci. Instrum.* **69**, 4221–4233 (1998).
12. H. Koizumi, Y. Yamashita, A. Maki, T. Yamamoto, Y. Ito, H. Itagaki, and R. Kennan, "Higher-order brain function analysis

- by trans-cranial dynamic NIRS imaging," *J. Biomed. Opt.* **4**, 403–413 (1999).
13. J. P. Van Houten, D. A. Benaron, S. Spilman, and D. K. Stevenson, "Imaging brain injury using time-resolved near infrared light scanning," *Pediatr. Res.* **39**, 470–476 (1996).
 14. H. Eda, I. Oda, Y. Ito, Y. Wada, Y. Oikawa, Y. Tsunazawa, M. Takada, Y. Tsuchiya, Y. Yamashita, M. Oda, A. Sassaroli, Y. Yamada, and M. Tamura, "Multichannel time-resolved optical tomographic imaging system," *Rev. Sci. Instrum.* **70**, 3595–3602 (1999).
 15. H. Rinneberg, D. Grosenick, H. Wabnitz, H. Danlewski, K. Moesta, and P. Schlag, "Time-domain mammography: results on phantoms, healthy volunteers, and patients," in *Advances in Optical Imaging and Photon Migration*, J. G. Fujimoto and M. S. Patterson, eds., Vol. 21 of OSA Trends in Optics and Photonics Series (Optical Society of America, Washington, D.C., 1998), pp. 278–280.
 16. H. Jiang, K. D. Paulsen, U. L. Osterberg, B. W. Pogue, and M. S. Patterson, "Simultaneous reconstruction of optical absorption and scattering maps in turbid media from near-infrared frequency-domain data," *Opt. Lett.* **20**, 2128–2130 (1995).
 17. M. Kaschke, H. Jess, G. Gaida, J.-M. Kaltenbach, and W. Wrobel, "Transillumination imaging of tissue by phase modulation techniques," in *Advances in Optical Imaging and Photon Migration*, J. G. Fujimoto and M. S. Patterson, eds., Vol. 21 of OSA Trends in Optics and Photonics Series (Optical Society of America, Washington, D.C., 1998), pp. 88–92.
 18. B. Chance, M. Cope, E. Gratton, N. Ramanujam, and B. Tromberg, "Phase measurement of light absorption and scatter in human tissue," *Rev. Sci. Instrum.* **69**, 3457–3481 (1998).
 19. F. E. W. Schmidt, M. E. Fry, E. M. C. Hillman, J. C. Hebden, and D. T. Delpy, "A 32-channel time-resolved instrument for medical optical tomography," *Rev. Sci. Instrum.* **71**, 256–265 (2000).
 20. J. C. Hebden, F. E. W. Schmidt, M. E. Fry, M. Schweiger, E. M. C. Hillman, and D. T. Delpy, "Simultaneous reconstruction of absorption and scattering images by multichannel measurement of purely temporal data," *Opt. Lett.* **24**, 534–536 (1999).
 21. M. Firbank, M. Oda, and D. T. Delpy, "An improved design for a stable and reproducible phantom material for use in near-infrared spectroscopy and imaging," *Phys. Med. Biol.* **40**, 955–960 (1995).
 22. M. Schweiger and S. R. Arridge, "Application of temporal filters to time resolved data in optical tomography," *Phys. Med. Biol.* **44**, 1699–1717 (1999).
 23. E. M. C. Hillman, J. C. Hebden, F. E. W. Schmidt, S. R. Arridge, M. S. Schweiger, H. Dehghani, and D. T. Delpy, "Calibration techniques and data type extraction for time-resolved optical tomography," *Rev. Sci. Instrum.* (to be published).
 24. M. Schweiger and S. R. Arridge, "Comparison of two- and three-dimensional reconstruction methods in optical tomography," *Appl. Opt.* **37**, 7419–7428 (1998).
 25. S. R. Arridge and M. Schweiger, "A gradient-based optimization scheme for optical tomography," *Opt. Express* **2**, 213–226 (1998), <http://www.osa.org/epubs/opticsexpress>.
 26. S. R. Arridge, M. Schweiger, M. Hiraoka, and D. T. Delpy, "Performance of an iterative reconstruction algorithm for near infrared absorption and scatter imaging," in *Photon Migration and Imaging in Random Media and Tissues*, B. Chance and R. R. Alfano, eds., *Proc. SPIE* **1888**, 360–371 (1993).
 27. S. R. Arridge, J. C. Hebden, M. Schweiger, F. E. W. Schmidt, M. E. Fry, E. M. C. Hillman, H. Dehghani, and D. T. Delpy, "A method for 3-D time-resolved optical tomography," *Int. J. Imaging Syst. Technol.* (to be published).